



# Impact of the uniaxial strain on terahertz modulation characteristics in flexible epitaxial VO<sub>2</sub> film across the phase transition

XUE CHANG,<sup>1,2</sup> JIANG LI,<sup>2</sup>  JIAN MU,<sup>2</sup> CHUN-HAO MA,<sup>3</sup>  
WANXIA HUANG,<sup>1</sup> HONG-FU ZHU,<sup>1,2</sup> QIAO LIU,<sup>2</sup> LIANG-HUI DU,<sup>2</sup>  
SEN-CHENG ZHONG,<sup>2</sup> ZHAO-HUI ZHAI,<sup>2</sup> SUJIT DAS,<sup>4</sup>  
YEN-LIN HUANG,<sup>3</sup> GANG-BEI ZHU,<sup>2</sup> LI-GUO ZHU,<sup>2,5</sup>  
AND QIWU SHI<sup>1,6</sup> 

<sup>1</sup>College of Materials Science and Engineering, Sichuan University, Chengdu, Sichuan 610065, China

<sup>2</sup>Institute of Fluid Physics, China Academy of Engineering Physics, Mianyang, Sichuan 621900, China

<sup>3</sup>Department of Materials Science and Engineering, National Yang Ming Chiao Tung University, Hsinchu, Taiwan 30010, China

<sup>4</sup>Material Research Centre, Indian Institute of Science, Bangalore 560012, India

<sup>5</sup>zhuliguo@tsinghua.org.cn

<sup>6</sup>shiqiwu@scu.edu.cn

**Abstract:** Exploring flexible electronics is on the verge of innovative breakthroughs in terahertz (THz) communication technology. Vanadium dioxide (VO<sub>2</sub>) with insulator-metal transition (IMT) has excellent application potential in various THz smart devices, but the associated THz modulation properties in the flexible state have rarely been reported. Herein, we deposited an epitaxial VO<sub>2</sub> film on a flexible mica substrate via pulsed-laser deposition and investigated its THz modulation properties under different uniaxial strains across the phase transition. It was observed that the THz modulation depth increases under compressive strain and decreases under tensile strain. Moreover, the phase-transition threshold depends on the uniaxial strain. Particularly, the rate of the phase transition temperature depends on the uniaxial strain and reaches approximately 6 °C/% in the temperature-induced phase transition. The optical trigger threshold in laser-induced phase transition decreased by 38.9% under compressive strain but increased by 36.7% under tensile strain, compared to the initial state without uniaxial strain. These findings demonstrate the uniaxial strain-induced low-power triggered THz modulation and provide new insights for applying phase transition oxide films in THz flexible electronics.

© 2023 Optica Publishing Group under the terms of the [Optica Open Access Publishing Agreement](#)

## 1. Introduction

The THz frequency region of the electromagnetic spectrum has attracted considerable attention because of its huge application potential in next-generation communication technology. For this vision, THz smart devices, such as but not limited to modulators and switching, need to be explored urgently, and many advanced materials for these purposes have emerged [1–4]. The rapid development of flexible electronics has been proposed to be fundamental for smart communication technologies, wherein the most exciting vision is called the Internet of Thing (IoT). Flexible electronics, such as wearable devices, implantable medical devices, electronic skin, and intelligent electronic fabrics, have been proposed as part of the blueprint for future human life [5–8]. In turn, there is a high demand for developing flexible and tunable THz devices based on new materials and concepts.

Several materials have been proposed to develop flexible THz devices, such as conductive polymers [9], two-dimensional materials [10], and liquid crystals [11]. However, the lack of THz modulation depth, operation speed, and insertion loss is yet to be resolved. As a typical

phase change material, vanadium dioxide ( $\text{VO}_2$ ) undergoes a reversible IMT near 341 K, with the resistivity changing sharply by 4-5 orders of magnitude [12–16]. The IMT occurs at an ultrafast time scale and can be triggered by multiple approaches, such as thermal [16–18], electrical [19], optical [20–23], and strain stimuli [24]. These characteristics make  $\text{VO}_2$  an intriguing material for use in tunable THz devices. In particular, the compatibility of  $\text{VO}_2$  with metamaterials has been explored to realize various THz smart devices, including switching, amplitude modulation, phase modulation, and sensing [25–31]. However, the growth of  $\text{VO}_2$  always requires a high-temperature condition (400–600 °C) for the nucleation and stoichiometric evolution of  $\text{VO}_2$  (owing to the multiple valence characteristics of vanadium). Therefore,  $\text{VO}_2$  films for THz devices are generally deposited on rigid substrates such as  $\text{TiO}_2$  [17], sapphire [32], or  $\text{SiO}_2$  [33]. Thus, developing flexible THz devices based on  $\text{VO}_2$  is a great challenge because most flexible substrates, such as polymers, cannot withstand high temperatures.

Recently, a lift-off strategy has been proposed for realizing flexible  $\text{VO}_2$  films. The film can be released from the substrate by etching a sacrificial layer between the film and substrate and then transferring it onto a flexible substrate. For example, Li *et al.* recently lifted an epitaxial  $\text{VO}_2$  film from the substrate using a ZnO sacrificial layer and realized a high-quality freestanding  $\text{VO}_2$  membrane with a large size of 900 mm<sup>2</sup> [34]. Han *et al.* reported that ultrathin  $\text{VO}_2$  films were detached from the substrate by dissolving a  $\text{Sr}_3\text{Al}_2\text{O}_6$  sacrificial layer [35]. Nevertheless, the lift-off method always requires a long reaction time in the etching solution, and the transfer process should be controlled carefully to ensure the integrity of the films and avoid cracks or breakages [34–36]. In response to these challenges, it has been proposed that the growth of  $\text{VO}_2$  films directly on mica substrates would be more promising for preparing flexible  $\text{VO}_2$  films [37,38]. Mica substrates are highly flexible, chemically stable, and tolerant to high temperatures. Moreover, it has been demonstrated that  $\text{VO}_2$  can be grown directly on mica substrates via van der Waals (vdW) epitaxy, which mitigates misfit strain and substrate clamping for flexible electronics applications [39–42]. Thus, it has great potential for developing flexible and smart electronic devices based on  $\text{VO}_2$  films. For example, Li *et al.* successfully fabricated a flexible  $\text{VO}_2$  film on a high-tolerance mica substrate and used it for in-sensor computing applications with ultraviolet light [26]. Wang *et al.* demonstrated an infrared meta-absorber with mechanical flexibility and electrical tunability based on a  $\text{VO}_2$  film on a flexible mica sheet [18]. However, the investigation of flexible  $\text{VO}_2$  films in the THz range has not yet been reported. In particular, the THz modulation properties and excitation power for triggering the phase transition are the most important parameters for applying flexible  $\text{VO}_2$  films in smart THz devices.

In this work, we fabricated epitaxial  $\text{VO}_2$  films on a mica substrate by pulsed laser deposition and investigated their THz transmission properties under uniaxial tensile strain and compressive strain across temperature-induced and laser-induced phase transitions. It can be observed that the uniaxial strain affected the THz modulation depth and the phase transition threshold of the flexible  $\text{VO}_2$  films. In the temperature-induced phase transition process, the modulation depth could be tuned from 80.1% under compressive strain (-0.48%) to 71.3% under tensile strain (0.48%). In addition, the phase transition temperature decreased under compressive strain but increased under tensile strain. More interestingly, compared to the initial state, the optical trigger threshold is reduced by 38.9% under compressive strain, whereas it is increased by 36.7% under tensile strain in the laser-induced phase transition. Using this method, we can design flexible  $\text{VO}_2$  films with excellent THz modulation properties but a low-power triggered superiority in the phase transition. Therefore, this would promote  $\text{VO}_2$ -based flexible THz devices.

## 2. Experimental section

### 2.1. Sample preparation

We used a  $\text{V}_2\text{O}_5$  target to deposit the  $\text{VO}_2$  film on the (001) native mica substrate by pulsed laser deposition with a KrF excimer laser ( $\lambda = 248$  nm, coherent) operated at a laser repetition rate of

10 Hz for 20 min and a laser fluence of 1 J/cm<sup>2</sup>. The deposition was conducted at 5 mTorr oxygen, and the substrates were heated to 650 °C. The thickness of the VO<sub>2</sub> thin films was approximately 122 nm. The thickness of mica was approximately 40 μm. The dimensions of the samples were 6 × 7 mm.

## 2.2. Characterization

The phase compositions of the deposited films were characterized by X-ray diffraction (XRD). X-ray photoelectron spectroscopy (XPS) was used to get core-level spectra of the VO<sub>2</sub> layer (depth within 10 nm) with Thermo K-alpha XPS System from Thermo Fisher (ESCALAB 250 Xi, USA) with a base pressure better than 8.0 × 10<sup>-3</sup> Pa employing a monochromatic Al Kα radiation source (hν=1486.6 eV). Transmission electron microscopy (TEM) was used to confirm the crystal structure and quality of the interfaces. A typical THz time-domain spectroscopy (THz-TDS) was used to measure the THz modulation properties of the VO<sub>2</sub> film under strain during temperature-induced IMT. The samples were mounted on an mK2000 temperature controller, which offers precision, accuracy, and stability for the temperature measurements. Time-resolved terahertz spectroscopy (TRTS) (see Supplement 1 for details) is used for researching the laser-induced phase transition of the VO<sub>2</sub>/mica film under strain. Briefly, a 1-mJ, 100 fs laser at 800 nm with a 500 Hz repetition rate was used in this system. The laser was separated into three beams, one of which was frequency-doubled to 400 nm and mixed with the fundamental 800 nm pulse to generate broadband THz light in nitrogen-purged air. The second 800 nm beam was chirped and combined with THz light to produce a visible probe light by a third-order nonlinear process called four-wave mixing ( $\omega_1 + \omega_1 - \omega_{\text{THz}} = \omega_2$ ). The up-conversion of visible probe light was recorded using an optical spectrometer with an Andor EMCCD (Oxford Instruments). Then, nonlinear spectral up-conversion was achieved, allowing direct detection across the entire source spectral range in the frequency domain without Fourier transformation. The third 800 nm beam served as the pump light to excite the IMT process of the VO<sub>2</sub> film (see Supplement 1 for details). In the strain-dependent optical-pump TRTS measurement, the terahertz beam spot was 0.2 mm, while the optical beam spot was 0.5 mm. The optical pump and the terahertz beam were both impinged at normal incidence. The entire THz beam path was purged with high-purity nitrogen to prevent water vapor absorption.

## 3. Results and discussion

To examine the phase compositions and structural information of VO<sub>2</sub>/mica heteroepitaxy, a typical XRD, XPS, and TEM (see Supplement 1 for details) were used. These results indicate the high crystalline quality of thin films without secondary phases. In addition, a defect-free and non-coherent interface implies the presence of a weak interaction between the two materials, validating vdW epitaxy in the VO<sub>2</sub>/mica heterostructure.

When the VO<sub>2</sub>/mica heterostructure is compressed or stretched out of equilibrium, strain is generated. The stiffness tensor provides the constitutive relationship between the stress and the final strain state. The external uniaxial strain of the VO<sub>2</sub>/mica film in the bent state was calculated using the following formula [43]:

$$\varepsilon = \pm \frac{y/2 + t}{R} \times 100\%, \quad (1)$$

where  $R$ ,  $y$ , and  $t$  represent the bending radius, substrate thickness, and thin film thickness, respectively. Figure 1(a) shows a schematic of the VO<sub>2</sub> film under tensile and compressive strains. In particular, the film is subjected to tensile strains when the obverse of the VO<sub>2</sub>/mica film is upward on the bending equipment, where  $\varepsilon$  is a positive value, while the reverse of the VO<sub>2</sub>/mica film is upward on the bending equipment, where  $\varepsilon$  is a negative value representing compressive strain. The VO<sub>2</sub>/mica film strain was measured while maintaining the bending state. The external

uniaxial strain values of the VO<sub>2</sub> film under various bending radii are shown in Fig. 1(b). The theoretical value of the external strain applied to the plane of the VO<sub>2</sub>/mica heterostructures was 0.24% with a bending radius of 8.3 mm and 0.48% with a bending radius of 4.16 mm. The external bending equipment in the inset of Fig. 1(b) was made of aluminum for good thermal conductivity and had dimensions of 40 × 16 × 15 mm<sup>3</sup>. A small square hole with a side length of 5 mm at the center was used for THz transmittance measurements. Figure 1(c) shows an optical image of the flexible VO<sub>2</sub> film on the mica substrate, reflecting the excellent flexibility of the film.

We observed a uniaxial strain-dependent THz modulation depth for the flexible VO<sub>2</sub> film across the temperature-induced phase transition using the THz-TDS system. The THz transmission properties of the VO<sub>2</sub> film were investigated in the temperature range of 25-95 °C. As shown in Fig. 2(a)-(c), the THz time-domain transmission signals exhibited an obvious temperature dependence. In particular, the decreased transmission amplitude with temperature indicates an insulator-metal phase transition during heating, and the increased transmission amplitude with temperature proves the metal-insulator phase recovery during the cooling process (see Supplement 1 for details). In addition, we obtained the frequency-domain transmission amplitude for the VO<sub>2</sub> thin films during the heating process (from 25 °C to 95 °C) under different axial strains (see Supplement 1 for details). Moreover, the phase transition characteristics can be observed under different uniaxial strains, from compressive (-0.48%) to tensile (0.48%). Based on multiple sets of experiments and the recording of transmittance signals across the phase transition, we obtained the THz modulation depth of the film under different uniaxial strains, as shown in Fig. 2(d). Here, the THz modulation depth ( $Md$ ) was calculated as  $Md = \frac{E_I(t) - E_M(t)}{E_I(t)} \times 100\%$ , where  $E_I(t)$  and  $E_M(t)$  are the THz electric fields transmitted through the VO<sub>2</sub> film at the insulator phase and metallic phases, respectively. The THz modulation depth shows a downward trend with the tensile strain and an upward trend with the compressive strain. In detail,  $Md$  is 80.1% for the film under a uniaxial strain of -0.48% (compressive) and 71.3% for the film under a uniaxial strain of 0.48% (tensile).

The effect of uniaxial strain on the THz modulation properties of the flexible film was further investigated by evaluating the THz transmittance under different uniaxial strains before and after the phase transition. The frequency-domain spectra and normalized THz transmission spectra as a function of frequency for the VO<sub>2</sub> film under different uniaxial strains across the phase transition were obtained (see Supplement 1 for details). Figure 3(a) shows the normalized THz transmission amplitude for the film before (25 °C) and after (95 °C) the phase transition under different uniaxial strains from -0.48 to 0.48%. The result indicates nearly the same THz transmission of approximately 90% under different uniaxial strains before phase transition. However, the transmission amplitude decreased with compressive strain but increased continuously with tensile strain after phase transition. This result is consistent with the THz modulation depth shown in Fig. 2(d).

To obtain deeper insights into the impact of strain on the phase-transition characteristics of the flexible VO<sub>2</sub> epitaxial film, we extracted the transient THz conductivity of the VO<sub>2</sub> film under different uniaxial strains during the IMT dynamic process. Specifically, the frequency-dependent real and imaginary parts of the THz conductivity spectrum of VO<sub>2</sub> films under different axial strains during the temperature-induced phase transition (see Supplement 1 for details) is directly proportional to the strain-induced THz electric field transmission using the following equation [44]:

$$\frac{E_{sub}(w)}{E_{sam}(w)} = \frac{n_{Air} + n_{sub}}{n_{Air} + n_{sub} + Z_0\sigma(w)l}, \quad (2)$$

where  $E_{sub}(w)$  and  $E_{sam}(w)$  represent the THz transmission amplitudes of the bare substrate and the sample, respectively.  $n_{Air}$  is the refractive index of air, equal to 1, and the refractive index of the substrate in the THz range determined by our THz-TDS is approximately 1.58. The thickness of the film is approximately 122 nm, and the impedance of the free space is  $Z_0 = 377$

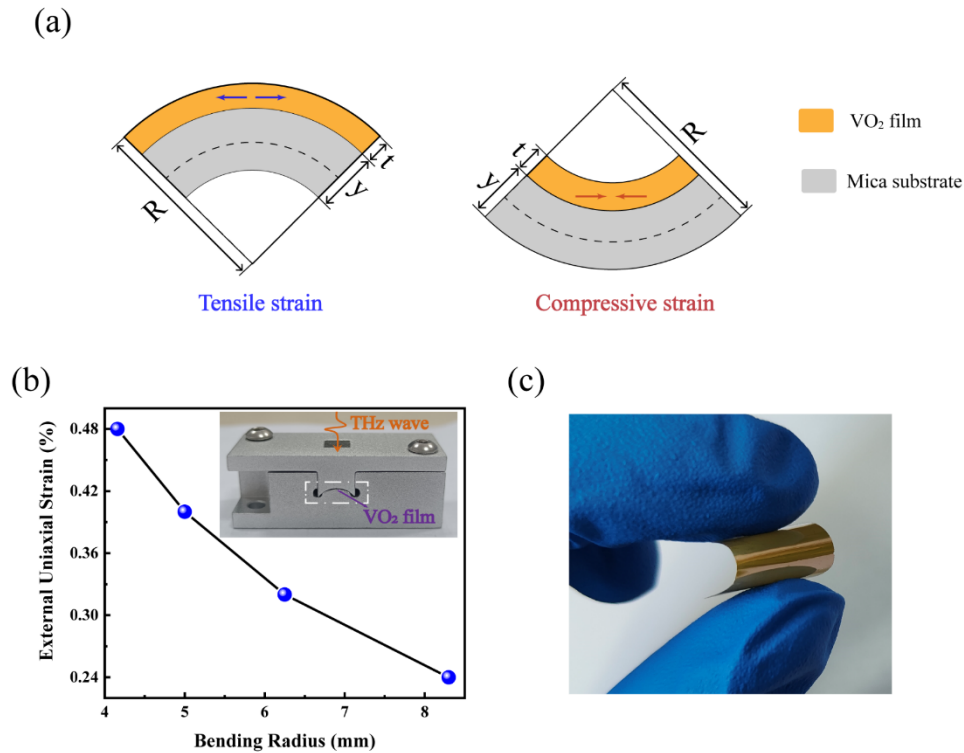


**Fig. 1.** (a) Schematic of the sample under tensile and compressive strains, where  $R$  is the bending radius,  $y$  is the thickness of the mica substrate, and  $t$  is the thickness of the VO<sub>2</sub> film (the blue arrows represent tensile strain and the red arrows represent compressive strain). (b) External uniaxial strain in the VO<sub>2</sub> films under various bending radii. The inset shows the schematic of the bending equipment. (c) Optical image of the flexible VO<sub>2</sub> film on the mica substrate.

$\Omega$ . Figure 3(b) shows the magnitude of the real part of the THz conductivity [ $\sigma_{real}(w)$ ] as a function of the external uniaxial strain across the phase transition (from 25 °C to 95 °C), which is calculated at 0.42 THz. It can be clearly seen that the THz conductivity has very little discrepancy under uniaxial strain before the phase transition but increases with compressive strain, while it decreases with tensile strain after the phase transition. Thus, it can account for lower THz transmission under compressive strain, but higher THz transmission under tensile strain. This phenomenon has been reported in VO<sub>2</sub> nanobeams under different external strains: the resistance increased with tensile stress, while it decreased with compressive strain [27]. Lattice compression usually increases orbital overlap and electronic bandwidth [45]. In the insulator state, the  $\pi_*$  orbitals lie above the Fermi level (EF), and electron transfer is not expected owing to the relatively small changes in the lattice parameters. In contrast, strain-dependent orbital occupation changes are significant in the metallic state. Remarkably, this implies that the orbital occupation of the metallic state is directly related to the applied uniaxial strain [13].

The temperature-induced phase transition of the flexible epitaxial VO<sub>2</sub> film was observed by recording the hysteresis loop of the normalized THz transmission vs. temperature. As shown in Fig. 4(a)-(c), the film under different uniaxial strain states exhibits a drastic decrease in THz transmission during heating but recovery of THz transmission during cooling, corresponding to the IMT and metal-insulator phase recovery, respectively. The phase transition temperature could be obtained according to the derivatives of the temperature dependence of THz transmission that



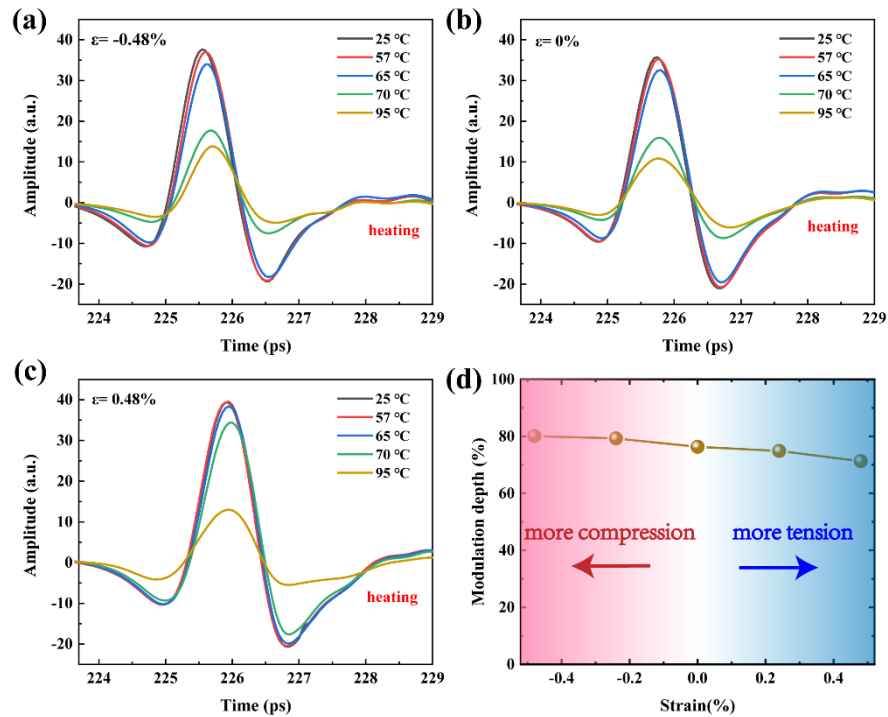


**Fig. 2.** THz transmission properties of the VO<sub>2</sub> film on mica under strain and temperature. (a–c) Strain and temperature dependences of the THz time-domain transmission signals of the VO<sub>2</sub>/mica heterostructures during heating processes. (d) THz modulation depth of the VO<sub>2</sub> film under different uniaxial strains.

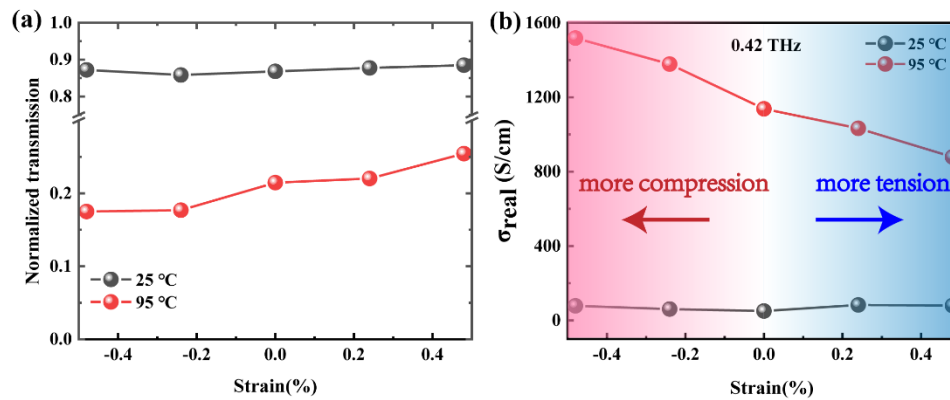


**Fig. 3.** THz transmission spectra and photoconductivity spectra of VO<sub>2</sub> film under strain. (a) THz transmission spectra under different uniaxial strains from -0.48 to 0.48% across the phase transition at the temperature range from 25 to 95 °C. (b) Real part of photoconductivity spectra under different uniaxial strains before (25 °C) and after phase transition (95 °C), which is calculated at 0.42 THz.

were extracted from each of the hysteresis loops (Insets in Fig. 4(a)-(c)). Figure 4(d) shows the IMT temperature as a function of the external uniaxial strain in the THz region. In particular, the IMT temperature increased linearly from compressive strain to tensile strain with slopes of approximately  $6.0\text{ }^{\circ}\text{C per \%}$  during both heating and cooling processes. Here, the strain imposed on the flexible  $\text{VO}_2$  film followed the process: original state  $\rightarrow$  compressive  $\rightarrow$  release  $\rightarrow$  tension  $\rightarrow$  release). The results indicate the repeatable and stable performance of the film when subjected to cyclic stretching and compression. Our experimental results are consistent with theoretical predictions based on first-principles calculations [46]. In the compressive state, the rutile c-axis ( $c_R$ ) decreases with the increase in compressive strain, which promotes the phase change of the  $\text{VO}_2$  film and leads to a decreased IMT threshold. In contrast, there is an increase in  $c_R$  with an increase in the tensile strain. Therefore, the IMT dynamic process of the  $\text{VO}_2$  film was obstructed, resulting in an increased IMT threshold [13,27,43].

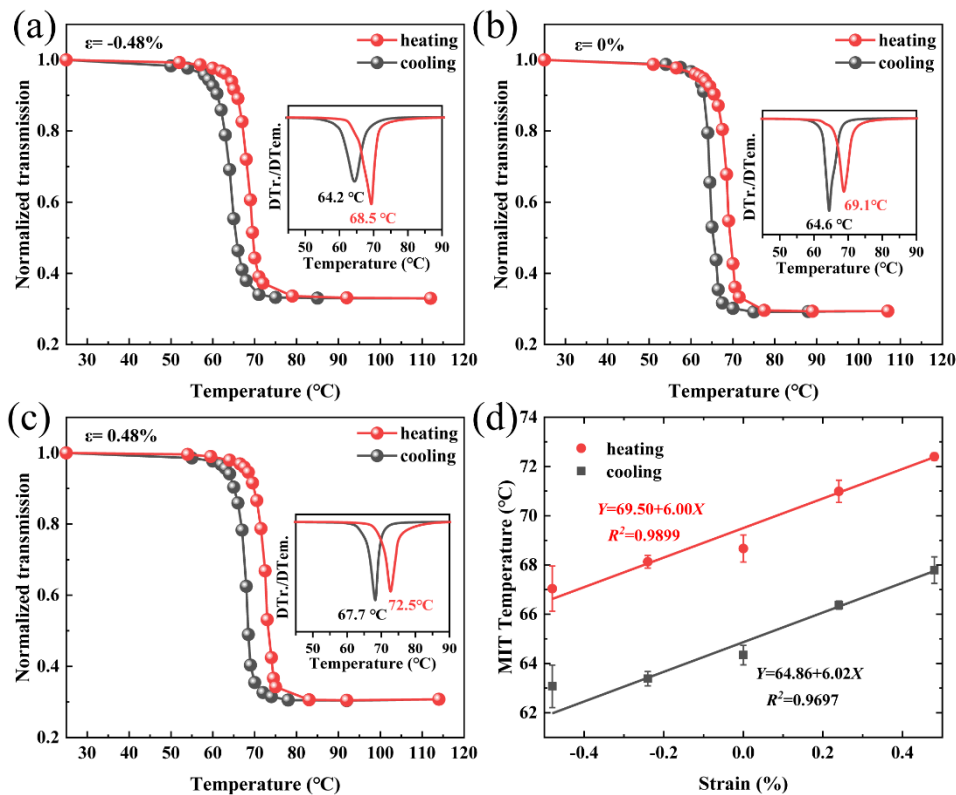


**Fig. 4.** Thermal effect on the transmission under the strain of the  $\text{VO}_2/\text{mica}$  heterostructures. (a-c) Thermal hysteresis loop of the normalized transmission against temperature under different uniaxial strains and the corresponding derivative of transmission for the heating (red) and cooling transition curves (black). The  $\text{VO}_2$  film undergoes strain processes (original state  $\rightarrow$  compressive  $\rightarrow$  release  $\rightarrow$  tension  $\rightarrow$  release). (d) Analysis of the IMT temperatures as a function of external uniaxial strain.

The phase transition process of the flexible  $\text{VO}_2$  film was investigated using optical-pump TRTS system. Figure 5(a) shows a schematic representation of the optically controlled flexible epitaxial  $\text{VO}_2$  film. The dynamic processes of the THz electric field changes ( $|\Delta E/E_0|$ ) in the flexible  $\text{VO}_2$  film under different uniaxial strains at a pump fluence of  $6.4\text{ mJ/cm}^2$  are shown in Fig. 5(b).  $|\Delta E/E_0|$  as a function of delay time was well fitted with the bi-exponential function

$|\Delta E/E_0| = |A_1 \exp\left(\frac{-t}{\tau_1}\right) + A_2 \exp\left(\frac{-t}{\tau_2}\right) + B|$ , where  $A_1$  and  $A_2$  correspond to the amplitudes of the fast non-thermal IMT process and the slow process of metallic phase propagation into the interior of the VO<sub>2</sub> film, respectively.  $\tau_1$  and  $\tau_2$  correspond to the fast non-thermal IMT process and the slow process of metallic phase propagation into the interior of the VO<sub>2</sub> film, respectively [47,48,49,50]. Here,  $E_0$  is the amplitude of the electric field of the THz signal transmitted through the VO<sub>2</sub> film without the laser pump, and  $\Delta E$  is the THz electric field change before and after the phase transition owing to the laser pump. In the strain-dependent optical-pump terahertz-probe measurement, the THz electric field changes ( $|\Delta E/E_0|$ ) largely in a time scale of a few picoseconds triggered by the laser with a pump fluence of 6.4 mJ/cm<sup>2</sup>. This corresponds to the excellent IMT of the film. Moreover, Fig. 5(b) clearly indicates that the THz electric field change  $|\Delta E/E_0|$  for the film is dependent on the uniaxial strain. In addition, using  $Md = |\Delta E/E_0| \times 100\%$ , we obtained  $Md = 35.1\%$  for the VO<sub>2</sub>/mica film under a compressive strain of -0.48%,  $Md = 32.9\%$  for the VO<sub>2</sub>/mica film without uniaxial strain, and  $Md = 29.8\%$  for the VO<sub>2</sub>/mica film under a tensile strain of 0.48% at 400 ps. Particularly, the film under a compressive strain of -0.48% shows a larger THz modulation depth than that of the film without uniaxial strain. In contrast, the film under a tensile strain of 0.48% showed decreased THz modulation depth. This phenomenon has not yet been reported but is significant for smart THz devices based on flexible VO<sub>2</sub> films.

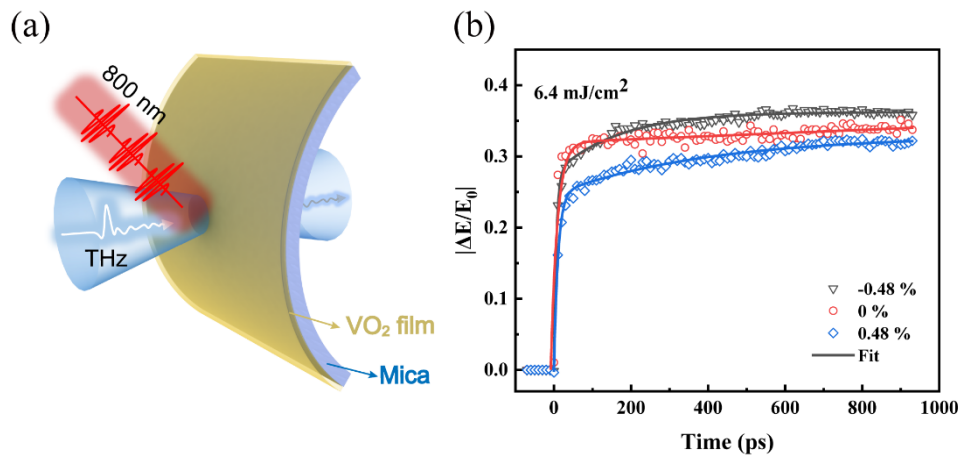


**Fig. 5.** (a) Schematic representation of optically controlled flexible epitaxial VO<sub>2</sub> film. (b) THz electric field changes ( $|\Delta E/E_0|$ ) of the flexible VO<sub>2</sub> thin film under different uniaxial strains ( $\epsilon = -0.48\%$ ,  $0\%$ , and  $0.48\%$ ) with pump fluence of 6.4 mJ/cm<sup>2</sup> at 6.5 THz (0 ps is the pumping point). The solid lines represent the fitting values using the bi-exponential function from the experiment data (dots).

The varied THz modulation behavior of the flexible VO<sub>2</sub> film under different uniaxial strains was further investigated by triggering the film with pump fluences from 4 to 16 mJ/cm<sup>2</sup>. Figure 6(a)–(c) shows that the ultrafast THz response can be distinguished from a fast process in 10–15 ps and a slow process in several tens of ps. This is consistent with the reported two-process phase transition of the VO<sub>2</sub> film revealed by the TRTS system. [30] Furthermore, the THz electric field change  $|\Delta E/E_0|$  increases gradually with the pump fluence, which refers to the enhanced phase transition amplitude under higher-energy laser excitation. To illustrate the free carrier excitation dynamics of the flexible VO<sub>2</sub> film under different uniaxial strains, we compared the THz electric field changes  $|\Delta E/E_0|$  of the film at the initial state ( $\epsilon = 0\%$ ) under a compressive strain of -0.48% and tensile strain of 0.48%, triggered by laser pump fluences. Figure 6(d) clearly



indicates that the THz electric field change increases under compressive strain and decreases under tensile strain, the same as observed in Fig. 2(b).

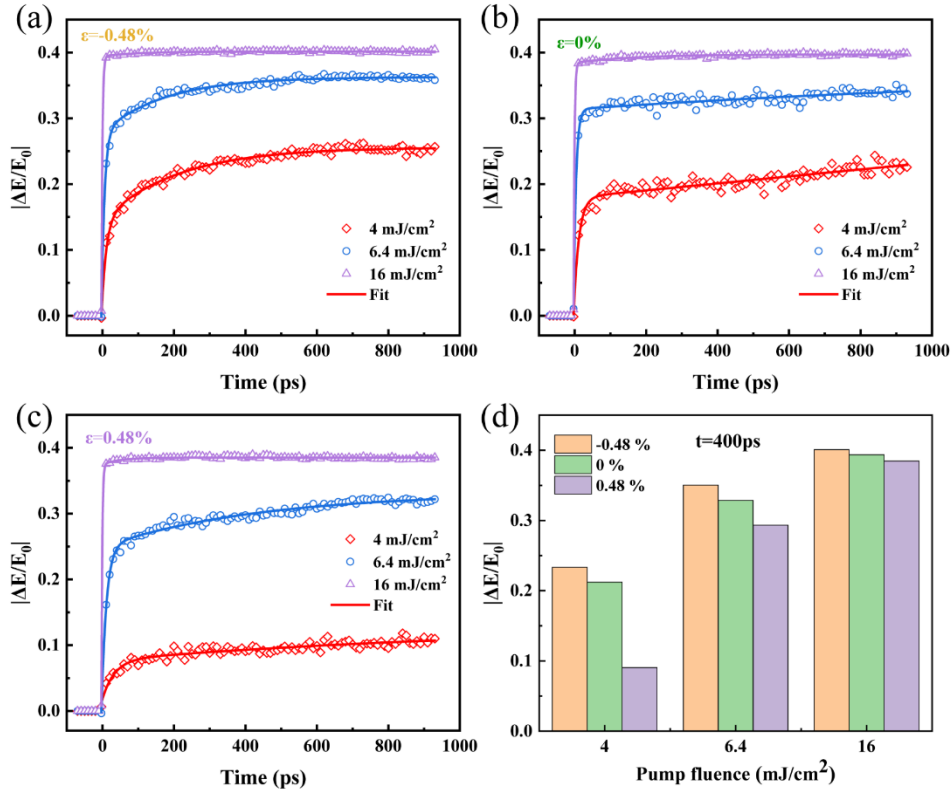


**Fig. 6.** (a-c) THz electric field changes ( $|\Delta E/E_0|$ ) of the flexible VO<sub>2</sub> thin film under different uniaxial strains ( $\epsilon = -0.48\%$ ,  $0\%$ , and  $0.48\%$ ) at different pump fluences (0 ps is the pumping point). d) Transient THz response of the film under different uniaxial strains ( $\epsilon = -0.48\%$ ,  $0\%$ , and  $0.48\%$ ) triggered with different pump delay times of 400 ps.

Furthermore, the epitaxial strain has been reported to be an efficient way to tune the phase-transition temperature of VO<sub>2</sub> deposited on a rigid substrate [13,51,52]. Here, we investigated the effect of compressive and tensile strains on the threshold for both temperature-induced and laser phase transitions of flexible epitaxial VO<sub>2</sub> films. Figure 7 shows the pump fluence dependence of the THz electric field changes  $|\Delta E/E_0|$  of VO<sub>2</sub>/mica under different uniaxial strains at a delay time of 400 ps at 6.5 THz. The optical trigger threshold for laser-induced phase transition ( $F_{\text{th}}$ ) is obtained via linearly fitting the rising segments of the THz electric field changes  $|\Delta E/E_0|$  versus pump fluence curves:  $F_{\text{th}} = 1.13$ ,  $F_{\text{th}} = 1.85$ , and  $F_{\text{th}} = 2.53 \text{ mJ}/\text{cm}^2$  for the compression state, original state and tension state of the VO<sub>2</sub>/mica, respectively.  $F_{\text{th}}$  for the VO<sub>2</sub>/mica film under compressive strain was substantially lower, approximately 38.9% of that for the initial VO<sub>2</sub>/mica film. In contrast,  $F_{\text{th}}$  for the VO<sub>2</sub>/mica film under tensile strain was substantially higher, approximately 36.7% of that for the original VO<sub>2</sub>/mica film. We also calculated the real transient THz photoconductivity of the flexible VO<sub>2</sub> film under different uniaxial strains at different pump fluences (see Supplement 1 for details) [53,54,55]. It can be seen that the real THz photoconductivity increases with compression while decreasing with tension for the same pump fluence.

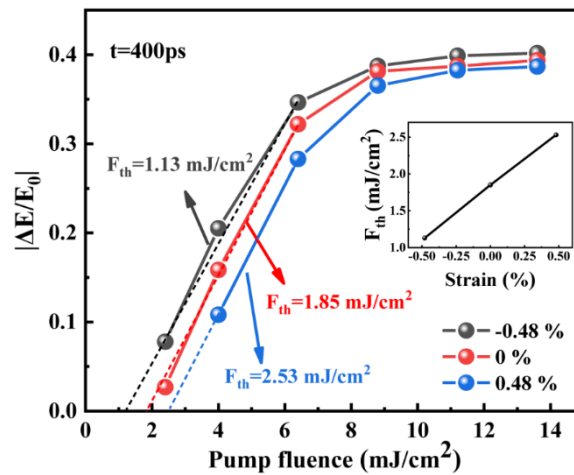


**Fig. 7.** Pump fluence dependence of the THz electric field changes ( $|\Delta E/E_0|$ ) of VO<sub>2</sub>/mica under different uniaxial strains at 400 ps delay times at 6.5 THz.  $F_{th}$  indicates the optical trigger threshold for laser-induced IMT. The inset shows the optical trigger threshold ( $F_{th}$ ) of the VO<sub>2</sub> film as a function of strains.

#### 4. Conclusion

In conclusion, we investigated the effect of uniaxial mechanical strain on the THz modulation properties of flexible VO<sub>2</sub> films grown epitaxially on mica substrates. The flexible film exhibits tunable THz modulation depth from 80.1 to 71.3% under different tension or compression states. Moreover, there was a pronounced strain-induced change in the phase-transition threshold of the flexible VO<sub>2</sub> film. Using this strategy, the phase transition temperature can decrease under compressive strain, and the pump fluence for laser-induced phase transition can be reduced by 38.9%. These findings demonstrate the THz modulation of flexible VO<sub>2</sub>/mica films through strain engineering and would provide fundamental insights into their applications in flexible THz smart devices.

**Funding.** National Natural Science Foundation of China (U2230128, U2030113, U20A20212); Sichuan Province Science and Technology Support Program (No. 2022NSFSC0498); the Fundamental Research Funds for Central Universities and the Distinguished Young Scholars of Sichuan Province (No. 2020JDJQ0008).

**Disclosures.** The authors declare no conflicts of interest related to this study.

**Data availability.** Data underlying the results presented in this paper are not publicly available at this time but may be obtained from the authors upon reasonable request.

**Supplemental document.** See [Supplement 1](#) for supporting content.

#### References

1. Z. Sun, A. Martinez, and F. Wang, "Optical modulators with 2D layered materials," *Nat. Photonics* **10**(4), 227–238 (2016).
2. K. Sengupta, T. Nagatsuma, and D. M. Mittleman, "Terahertz integrated electronic and hybrid electronic–photonic systems," *Nat. Electron.* **1**(12), 622–635 (2018).
3. R. I. Stantchev, B. Sun, S. M. Hornett, P. A. Hobson, G. M. Gibson, M. J. Padgett, and E. Hendry, "Noninvasive, near-field terahertz imaging of hidden objects using a single-pixel detector," *Sci. Adv.* **2**(6), e1600190 (2016).
4. Y. Yang, Y. Yamagami, X. Yu, P. Pitchappa, J. Webber, B. Zhang, M. Fujita, T. Nagatsuma, and R. Singh, "Terahertz topological photonics for on-chip communication," *Nat. Photonics* **14**(7), 446–451 (2020).
5. M. Wang, Y. Luo, T. Wang, C. Wan, L. Pan, S. Pan, K. He, A. Neo, and X. Chen, "Artificial Skin Perception," *Adv. Mater.* **33**(19), 2003014 (2021).
6. J. Park, Y. Lee, J. Hong, Y. Lee, M. Ha, Y. Jung, H. Lim, S. Y. Kim, and H. Ko, "Tactile-Direction-Sensitive and Stretchable Electronic Skins Based on Human-Skin-Inspired Interlocked Microstructures," *ACS Nano* **8**(12), 12020–12029 (2014).

7. Y. J. Yoo, S.-Y. Heo, Y. J. Kim, J. H. Ko, Z. F. Mira, and Y. M. Song, "Functional photonic structures for external interaction with flexible/wearable devices," *Nano Res.* **14**(9), 2904–2918 (2021).
8. Q. Xia, Y. Qin, P. Qiu, A. Zheng, and X. Zhang, "A bio-inspired tactile nociceptor constructed by integrating wearable sensing paper and a VO<sub>2</sub> threshold switching memristor," *J. Mater. Chem. B* **10**(12), 1991–2000 (2022).
9. Q. Shi, K. Tian, H. Zhu, Z.-R. Li, L.-G. Zhu, H. Deng, W. Huang, and Q. Fu, "Flexible and Giant Terahertz Modulation Based on Ultra-Strain-Sensitive Conductive Polymer Composites," *ACS Appl. Mater. Interfaces* **12**(8), 9790–9796 (2020).
10. L. Cheng, Z. Jin, Z. Ma, F. Su, Y. Zhao, Y. Zhang, T. Su, Y. Sun, X. Xu, Z. Meng, Y. Bian, and Z. Sheng, "Mechanical Terahertz Modulation Based on Single-Layered Graphene," *Adv. Opt. Mater.* **6**(7), 1700877 (2018).
11. X. Fu, L. Shi, J. Yang, Y. Fu, C. Liu, J. W. Wu, F. Yang, L. Bao, and T. J. Cui, "Flexible Terahertz Beam Manipulations Based on Liquid-Crystal-Integrated Programmable Metasurfaces," *ACS Appl. Mater. Interfaces* **14**(19), 22287–22294 (2022).
12. Z. Yang, C. Ko, and S. Ramanathan, "Oxide Electronics Utilizing Ultrafast Metal-Insulator Transitions," *Annu. Rev. Mater. Res.* **41**(1), 337–367 (2011).
13. N. B. Aetukuri, A. X. Gray, M. Drouard, M. Cossale, L. Gao, A. H. Reid, R. Kukreja, H. Ohldag, C. A. Jenkins, E. Arenholz, K. P. Roche, H. A. Dürr, M. G. Samant, and S. S. P. Parkin, "Control of the metal–insulator transition in vanadium dioxide by modifying orbital occupancy," *Nat. Phys.* **9**(10), 661–666 (2013).
14. C. Wu, F. Feng, and Y. Xie, "Design of vanadium oxide structures with controllable electrical properties for energy applications," *Chem. Soc. Rev.* **42**(12), 5157 (2013).
15. F. J. Morin, "Oxides Which Show a Metal-to-Insulator Transition at the Neel Temperature," *Phys. Rev. Lett.* **3**(1), 34–36 (1959).
16. G. Karaoglan-Bebek, M. N. F. Hoque, M. Holtz, Z. Fan, and A. A. Bernussi, "Continuous tuning of W-doped VO<sub>2</sub> optical properties for terahertz analog applications," *Appl. Phys. Lett.* **105**(20), 201902 (2014).
17. L. L. Fan, S. Chen, Z. L. Luo, Q. H. Liu, Y. F. Wu, L. Song, D. X. Ji, P. Wang, W. S. Chu, C. Gao, C. W. Zou, and Z. Y. Wu, "Strain Dynamics of Ultrathin VO<sub>2</sub> Film Grown on TiO<sub>2</sub> (001) and the Associated Phase Transition Modulation," *Nano Lett.* **14**(7), 4036–4043 (2014).
18. Z. Zheng, Y. Luo, H. Yang, Z. Yi, J. Zhang, Q. Song, W. Yang, C. Liu, X. Wu, and P. Wu, "Thermal tuning of terahertz metamaterial absorber properties based on VO<sub>2</sub>," *Phys. Chem. Chem. Phys.* **24**(15), 8846–8853 (2022).
19. J. Wang, B. Xiong, R. Peng, C. Li, B. Hou, C. Chen, Y. Liu, and M. Wang, "Flexible Phase Change Materials for Electrically-Tuned Active Absorbers," *Small* **17**(31), 2101282 (2021).
20. J. Jeong, N. Aetukuri, T. Graf, T. D. Schladt, M. G. Samant, and S. S. P. Parkin, "Suppression of Metal-Insulator Transition in VO<sub>2</sub> by Electric Field-Induced Oxygen Vacancy Formation," *Science* **339**(6126), 1402–1405 (2013).
21. A. Tognazzi, M. Gandolfi, B. Li, G. Ambrosio, P. Franceschini, R. Camacho-Morales, A. C. Cino, C. Baratto, D. de Ceglia, D. Neshev, and C. De Angelis, "Opto-thermal dynamics of thin-film optical limiters based on the VO<sub>2</sub> phase transition," *Opt. Mater. Express* **13**(1), 41 (2023).
22. C. Wan, E. H. Horak, J. King, J. Salman, Z. Zhang, Y. Zhou, P. Roney, B. Gundlach, S. Ramanathan, R. H. Goldsmith, and M. A. Kats, "Limiting Optical Diodes Enabled by the Phase Transition of Vanadium Dioxide," *ACS Photonics* **5**(7), 2688–2692 (2018).
23. V. R. Morrison, R. P. Chatelain, K. L. Tiwari, A. Hendaoui, A. Bruhács, M. Chaker, and B. J. Siwick, "A photoinduced metal-like phase of monoclinic VO<sub>2</sub> revealed by ultrafast electron diffraction," *Science* **346**(6208), 445–448 (2014).
24. J. Cao, E. Ertekin, V. Srinivasan, W. Fan, S. Huang, H. Zheng, J. W. L. Yim, D. R. Khanal, D. F. Ogletree, J. C. Grossman, and J. Wu, "Strain engineering and one-dimensional organization of metal–insulator domains in single-crystal vanadium dioxide beams," *Nat. Nanotechnol.* **4**(11), 732–737 (2009).
25. P. Markov, R. E. Marvel, H. J. Conley, K. J. Miller, R. F. Haglund, and S. M. Weiss, "Optically Monitored Electrical Switching in VO<sub>2</sub>," *ACS Photonics* **2**(8), 1175–1182 (2015).
26. G. Li, D. Xie, Z. Zhang, Q. Zhou, H. Zhong, H. Ni, J. Wang, E. Guo, M. He, C. Wang, G. Yang, K. Jin, and C. Ge, "Flexible VO<sub>2</sub> Films for In-Sensor Computing with Ultraviolet Light," *Adv. Funct. Mater.* **32**(29), 2203074 (2022).
27. B. Hu, Y. Ding, W. Chen, D. Kulkarni, Y. Shen, V. V. Tsukruk, and Z. L. Wang, "External-Strain Induced Insulating Phase Transition in VO<sub>2</sub> Nanobeam and Its Application as Flexible Strain Sensor," *Adv. Mater.* **22**(45), 5134–5139 (2010).
28. H.-F. Zhu, L.-H. Du, J. Li, Q.-W. Shi, B. Peng, Z.-R. Li, W.-X. Huang, and L.-G. Zhu, "Near-perfect terahertz wave amplitude modulation enabled by impedance matching in VO<sub>2</sub> thin films," *Appl. Phys. Lett.* **112**(8), 081103 (2018).
29. C. Ji, Z. Wu, X. Wu, H. Feng, J. Wang, Z. Huang, H. Zhou, W. Yao, J. Gou, and Y. Jiang, "Optimization of metal-to-insulator phase transition properties in polycrystalline VO<sub>2</sub> films for terahertz modulation applications by doping," *J. Mater. Chem. C* **6**(7), 1722–1730 (2018).
30. H. Ma, Y. Wang, R. Lu, F. Tan, Y. Fu, G. Wang, D. Wang, K. Liu, S. Fan, K. Jiang, and X. Zhang, "A flexible, multifunctional, active terahertz modulator with an ultra-low triggering threshold," *J. Mater. Chem. C* **8**(30), 10213–10220 (2020).
31. Z. Zheng, Y. Zheng, Y. Luo, Z. Yi, J. Zhang, Z. Liu, W. Yang, Y. Yu, X. Wu, and P. Wu, "A switchable terahertz device combining ultra-wideband absorption and ultra-wideband complete reflection," *Phys. Chem. Chem. Phys.* **24**(4), 2527–2533 (2022).
32. C. Chen, Y. Zhu, Y. Zhao, J. H. Lee, H. Wang, A. Bernussi, M. Holtz, and Z. Fan, "VO<sub>2</sub> multidomain heteroepitaxial growth and terahertz transmission modulation," *Appl. Phys. Lett.* **97**(21), 211905 (2010).

33. Y. Xiao, Z.-H. Zhai, Q.-W. Shi, L.-G. Zhu, J. Li, W.-X. Huang, F. Yue, Y.-Y. Hu, Q.-X. Peng, and Z.-R. Li, "Ultrafast terahertz modulation characteristic of tungsten doped vanadium dioxide nanogranular film revealed by time-resolved terahertz spectroscopy," *Appl. Phys. Lett.* **107**(3), 031906 (2015).
34. X. Li, Z. Yin, X. Zhang, Y. Wang, D. Wang, M. Gao, J. Meng, J. Wu, and J. You, "Epitaxial Lift-off of Wafer-Scale VO<sub>2</sub> Nanomembranes for Flexible, Ultrasensitive Tactile Sensors," *Adv. Mater. Technol.* **4**(7), 1800695 (2019).
35. K. Han, L. Wu, Y. Cao, H. Wang, C. Ye, K. Huang, H. Xing, X. Li, D.-C. Qi, X. Li, and X. Renshaw, "Enhanced metal-insulator transition in freestanding VO<sub>2</sub> down to 5 nm thickness," *ACS Appl. Mater. Interfaces* **13**(14), 16688–16693 (2021).
36. H. Ma, X. Xiao, Y. Wang, Y. Sun, B. Wang, X. Gao, E. Wang, K. Jiang, K. Liu, and X. Zhang, "Wafer-scale freestanding vanadium dioxide film," *Sci. Adv.* **7**(50), eabk3438 (2021).
37. X. Deng, Y.-F. Zhao, N. Zhong, F.-Y. Yue, R. Huang, H. Peng, X.-D. Tang, P.-H. Xiang, Y.-H. Chu, and C.-G. Duan, "Proton-Mediated Phase Control in Flexible and Transparent Mott Transistors," *Adv. Electron. Mater.* **6**(1), 1900742 (2020).
38. C.-I. Li, J.-C. Lin, H.-J. Liu, M.-W. Chu, H.-W. Chen, C.-H. Ma, C.-Y. Tsai, H.-W. Huang, H.-J. Lin, H.-L. Liu, P.-W. Chiu, and Y.-H. Chu, "van der Waal Epitaxy of Flexible and Transparent VO<sub>2</sub> Film on Muscovite," *Chem. Mater.* **28**(11), 3914–3919 (2016).
39. Y. Chen, L. Fan, Q. Fang, W. Xu, S. Chen, G. Zan, H. Ren, L. Song, and C. Zou, "Free-standing SWNTs/VO<sub>2</sub>/Mica hierarchical films for high-performance thermochromic devices," *Nano Energy* **31**, 144–151 (2017).
40. X. Deng, S. Wang, Y. Liu, N. Zhong, Y. He, H. Peng, P. Xiang, and C. Duan, "A Flexible Mott Synaptic Transistor for Nociceptor Simulation and Neuromorphic Computing," *Adv. Funct. Mater.* **31**(23), 2101099 (2021).
41. Y. He, H. Dong, Q. Meng, L. Jiang, W. Shao, L. He, and W. Hu, "Mica, a Potential Two-Dimensional-Crystal Gate Insulator for Organic Field-Effect Transistors," *Adv. Mater.* **23**(46), 5502–5507 (2011).
42. Y. Bitla and Y.-H. Chu, "van der Waals oxide heteroepitaxy for soft transparent electronics," *Nanoscale* **12**(36), 18523–18544 (2020).
43. H.-W. Chen, C.-I. Li, C.-H. Ma, Y.-H. Chu, and H.-L. Liu, "Strain engineering of optical properties in transparent VO<sub>2</sub>/muscovite heterostructures," *Phys. Chem. Chem. Phys.* **23**(14), 8908–8915 (2021).
44. H. Zhu, J. Li, L. Du, L. Shan, P. Li, X. Lu, T. Feng, S. Das, W. Huang, Q. Shi, and L. Zhu, "VO<sub>2</sub>-metallic hybrid metasurfaces for agile terahertz wave modulation by phase transition," *APL Mater.* **10**(3), 031112 (2022).
45. E. Arcangeletti, L. Baldassarre, D. D. Castro, S. Lupi, L. Malavasi, C. Marini, A. Perucchi, and P. Postorino, "Evidence of a Pressure-Induced Metallization Process in Monoclinic VO<sub>2</sub>," *Phys. Rev. Lett.* **98**(19), 196406 (2007).
46. Y. Cui, S. Shi, L. Chen, H. Luo, and Y. Gao, "Hydrogen-doping induced reduction in the phase transition temperature of VO<sub>2</sub>: a first-principles study," *Phys. Chem. Chem. Phys.* **17**(32), 20998–21004 (2015).
47. D. J. Hilton, R. P. Prasankumar, S. Fourmaux, A. Cavalleri, D. Brassard, M. A. E. Khakani, J. C. Kieffer, A. J. Taylor, and R. D. Averitt, "Erratum: Enhanced Photo susceptibility near T<sub>c</sub> for the Light-Induced Insulator-to-Metal Phase Transition in Vanadium Dioxide [Phys. Rev. Lett. 99, 226401 (2007)]," *Phys. Rev. Lett.* **100**(1), 019906 (2008).
48. B. T. O'Callahan, A. C. Jones, J. Hyung Park, D. H. Cobden, J. M. Atkin, and M. B. Raschke, "Inhomogeneity of the ultrafast insulator-to-metal transition dynamics of VO<sub>2</sub>," *Nat. Commun.* **6**(1), 6849 (2015).
49. X. Xue, M. Jiang, G. Li, X. Lin, G. Ma, and P. Jin, "Photoinduced insulator-metal phase transition and the metallic phase propagation in VO<sub>2</sub> films investigated by time-resolved terahertz spectroscopy," *J. Appl. Phys.* **114**(19), 193506 (2013).
50. S. Wall, D. Wegkamp, L. Foglia, K. Appavoo, J. Nag, R. F. Haglund, J. Stähler, and M. Wolf, "Ultrafast changes in lattice symmetry probed by coherent phonons," *Nat. Commun.* **3**(1), 721 (2012).
51. N. F. Quackenbush, H. Paik, and M. J. Wahila, *et al.*, "Stability of the M2 phase of vanadium dioxide induced by coherent epitaxial strain," *Phys. Rev. B* **94**(8), 085105 (2016).
52. Z. Shao, L. Wang, T. Chang, F. Xu, G. Sun, P. Jin, and X. Cao, "Controllable phase-transition temperature upon strain release in VO<sub>2</sub>/MgF<sub>2</sub> epitaxial films," *J. Appl. Phys.* **128**(4), 045303 (2020).
53. A. Kumar, A. Solanki, M. Manjappa, S. Ramesh, Y. K. Srivastava, P. Agarwal, T. C. Sum, and R. Singh, "Excitons in 2D perovskites for ultrafast terahertz photonic devices," *Sci. Adv.* **6**(8), eaax8821 (2020).
54. Y. Wang, F. Wang, G. Zhu, Q. Quan, Z. Lai, Y. Meng, Y. Fan, S. Yip, D. Zhao, and J. C. Ho, "Deconvoluting the energy transport mechanisms in all-inorganic CsPb<sub>2</sub>Br<sub>5</sub>/CsPbBr<sub>3</sub> perovskite composite systems," *APL Mater.* **10**(3), 031101 (2022).
55. G. R. Yettapu, D. Talukdar, S. Sarkar, A. Swarnkar, A. Nag, P. Ghosh, and P. Mandal, "Terahertz Conductivity within Colloidal CsPbBr<sub>3</sub> Perovskite Nanocrystals: Remarkably High Carrier Mobilities and Large Diffusion Lengths," *Nano Lett.* **16**(8), 4838–4848 (2016).